Synthesis of radiolabelled aryl azides from diazonium salts: experimental and computational results permit the identification of the preferred mechanism

Sameer M. Joshi, Abel de Cozar, Vanessa Gomez-Vallejo, Jacek Koziorowski, Jordi Llop and Fernando P. Cossio

Original Publication:

Sameer M. Joshi, Abel de Cozar, Vanessa Gomez-Vallejo, Jacek Koziorowski, Jordi Llop and Fernando P. Cossio, Synthesis of radiolabelled aryl azides from diazonium salts: experimental and computational results permit the identification of the preferred mechanism, 2015, Chemical Communications, (51), 43, 8954-8957.
http://dx.doi.org/10.1039/c5cc01913c

Journal Name

RSCPublishing

COMMUNICATION

Synthesis of Radiolabelled Aryl Azides from Diazonium Salts: Experimental and Computational Results Permit to Identify the Preferred Mechanism

Cite this: DOI: 10.1039/x0xx00000x

Received 00th January 2012,
Accepted 00th January 2012

DOI: 10.1039/x0xx00000x

www.rsc.org/

Sameer M. Joshi,[a] Abel de Cózar,[b,c,d,e] Vanessa Gómez-Vallejo,[f] Jacek Koziorowski,[g] Jordi Llop,[a,*] and Fernando P. Cossío[b,d,e*].

Experimental and computational studies on the formation of aryl azides from the corresponding diazonium salts support a stepwise mechanism via acyclic zwitterionic intermediates. The low energy barriers associated with both transition structures are compatible with very fast and efficient processes, thus making this method suitable for the chemical synthesis of radiolabelled aryl azides.

The use of organic azides, first prepared by Grieß in 1864,[1] ranges from the preparation of heterocycles, peptides[2] and pharmaceuticals,[3] to the synthesis of anilines and nitrenes.[4] The most prominent fields are currently Huisgen 1,3-dipolar azide-alkyne cycloadditions[5] and different variants of the Staudinger ligation.[6] Among organic azides, aryl azides have found industrial and biological application[7] in different fields due to their relatively high stability, and are important intermediates in organic chemistry.

Several approaches can be used for the preparation of aryl azides, including the reaction of diazonium salts with hydrazine,[8] *O*-benzylhydroxylamine hydrochloride[9] or azide ions.[10] Despite the latter reaction has been widely exploited for decades, its mechanism is still unclear and has been the subject to controversy.

In principle, at least three possible mechanisms can be predicted for this reaction. The first one consists of an Sn2Ar process similar to that observed for solvolysis reactions of diazonium salts,[11] as indicated in eq. (1):

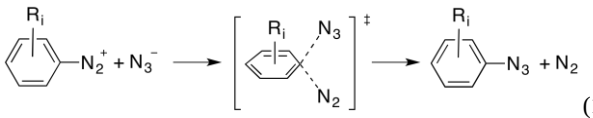

(1)

A second plausible mechanism involves a thermal (3+2) cycloaddition to form a 1*H*-pentazole cycloadduct[12] that, in turn, can yield the product via a second retro-(3+2) reaction:

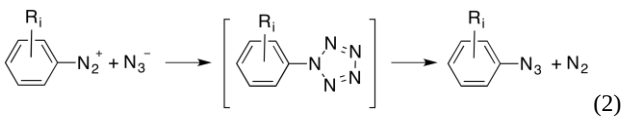

(2)

Finally, an addition-elimination process via an acyclic intermediate can be also considered, according to eq. (3):

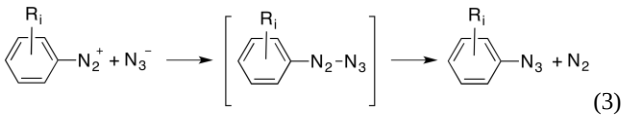

(3)

Previous studies[13] suggest that this latter mechanism is quite plausible. The process involves the attack of the azide on the diazonium ion with formation of aryl pentazenes and/or pentazoles, which subsequently lose nitrogen.[13] Whether the reaction occurs through a concerted (3+2) mechanism or takes place stepwise, and the nature of the intermediate products are questions that remain unresolved. Studies performed with ^{1}H and ^{15}N-NMR spectroscopy suggest the formation of three isomeric aryl pentazenes.[13] One of them would lead to the formation of the aryl azide directly, while the other two would require the formation of intermediate ring structures to finally yield the aryl azide.

Nitrogen-13 (^{13}N) is a positron emitter with a half-life of 9.97 minutes, and can be efficiently produced by proton irradiation of natural oxygen via the $^{16}O(p,\alpha)^{13}N$ nuclear reaction. When water is irradiated with 8-16 MeV protons, a mixture of $[^{13}N]NO_3^-$, $[^{13}N]NO_2^-$ and $[^{13}N]NH_4^+$ is obtained, being $[^{13}N]NO_3^-$ the major species (c.a. 85% of total radioactivity). $[^{13}N]NO_3^-$ can be quantitatively reduced to $[^{13}N]NO_2^-$ by passing $[^{13}N]NO_3^-$ over cadmium, and in our hands this labeling agent has proved useful for the synthesis of [^{13}N]nitrosamines,[14] [^{13}N]nitrosothiols[15] and [^{13}N]azo derivatives.[16]

In continuation of our work, and with the ultimate goal of synthesizing ^{13}N-labeled polysubstituted triazoles, we decided to approach the preparation of ^{13}N-labeled phenyl azides by adapting a

recently reported methodology,[17] based on the reaction of an aromatic amine with $NaNO_2$ and hydrazine hydrate (molar ratio 1:2:5) in the presence of acetic acid. According to the authors, one equivalent of sodium nitrite reacts with the aromatic amine to yield the corresponding diazonium salt; simultaneously, the reaction of another equivalent of nitrite with hydrazine hydrate generates *in situ* the azide ion, resulting in the formation of the aryl azide. When transitioning to radioactive conditions the reaction mechanism may have an impact on radiochemical yield. If the reaction proceeds via the mechanism shown in eq. (1), the radiolabelling information contained in the azide anion should be completely transferred to the corresponding aryl azide; however, if the radiolabelled diazonium salt is reacted with non-radioactive azide ion, labeled aryl azide would never be obtained. Similar reasoning can be applied to mechanisms shown in eqs. (2) and (3); hence the position of the label is paramount to prevent formation of $[^{13}N]N_2$ with the consequent decrease in labeling efficiency. With the aim of optimizing radiochemical yields, we envisaged a unique opportunity to further explore the mechanism of this reaction.

The synthetic process for the preparation of ^{13}N-labeled aryl azides was approached using two experimental settings (Scheme 1). In the first approach, denoted as A in Scheme 1, aniline was first reacted with sodium nitrite in the presence of hydrochloric acid, to yield the non-labeled diazonium salt (**1**). In a different vial, hydrazine hydrate was reacted with $[^{13}N]NO_2^-$ in the presence of acetic acid, to yield the ^{13}N-labeled azide ion (Scheme 1A). Both solutions were finally mixed in a capped vial to enable the formation of ^{13}N-labeled phenyl azide. In the second approach, denoted as B in Scheme 1, aniline was first reacted with $[^{13}N]NO_2^-$ in the presence of hydrochloric acid, to yield the ^{13}N-labeled diazonium salt ($[^{13}N]$**1**). In a different vial, hydrazine hydrate was reacted with sodium nitrite in the presence of acetic acid, to yield the non-labeled azide ion (Scheme 1B). Again, both solutions were finally mixed in a capped vial to enable the formation of ^{13}N-labeled phenyl azide.

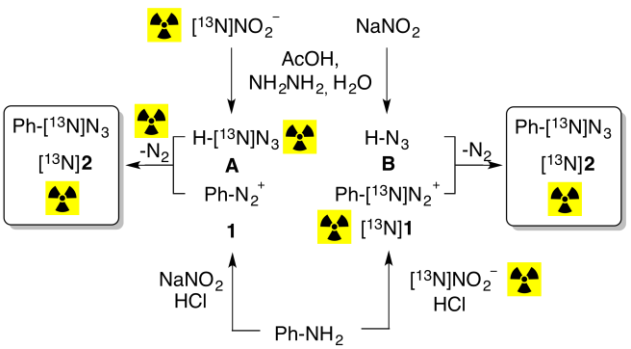

Scheme 1. The two alternative strategies A and B followed to synthesize ^{13}N-labeled phenyl azide ($[^{13}N]$**2**).

After termination of the reaction, the amount of radioactivity was measured with a dose calibrator (A_1), the vials were flushed with nitrogen to remove radioactive gases, the amount of radioactivity was measured again (A_2), and the reaction mixture was analyzed by HPLC using a radiometric detector in series with a UV detector. Identification of the ^{13}N-labeled azide was confirmed by co-elution with reference standard (see Electronic Supporting Information for further details).

Both synthetic strategies led to the formation of ^{13}N-labeled phenyl azide (**2**). However, the amount of radioactive gas generated during the reaction, determined as the difference between A_1 and A_2, and referred to the total amount of ^{13}N-labeled azide (the latter calculated as the product A_2 x A_{UC}, where A_{UC} is the area under the peak for phenyl azide as measured in the radiometric detector and expressed as percentage with respect to all integrated peaks in the chromatogram) was 100.3±1.7% and 4.0±1.1% for strategies A and B, respectively. Analysis of the flushed gas by radio-GC-MS showed the presence of a single radioactive peak, which was identified as $[^{13}N]N_2$, while the amount of labeled azide obtained in 1B was twice the amount obtained in A. These results confirm that approximately half of the radioactivity is lost as $[^{13}N]N_2$ when route A is followed, while the information of the radiolabel is almost quantitatively transferred to the azide under route B (Scheme 1).

The experimental data completely discard the reaction mechanism based on S_N2Ar (eq. 1) and cleavage of the C–heteroatom bond, which would lead to complete radioactivity loss (as $[^{13}N]N_2$) when route B is followed. On the other hand, they strongly suggest that the formation of the intermediate ring (eq. 2) is not taking place; in such a case, $[^{13}N]N_2$ would be detected in significant amount (c.a. 100% with respect to the final amount of labelled aryl azide) when route B was used.

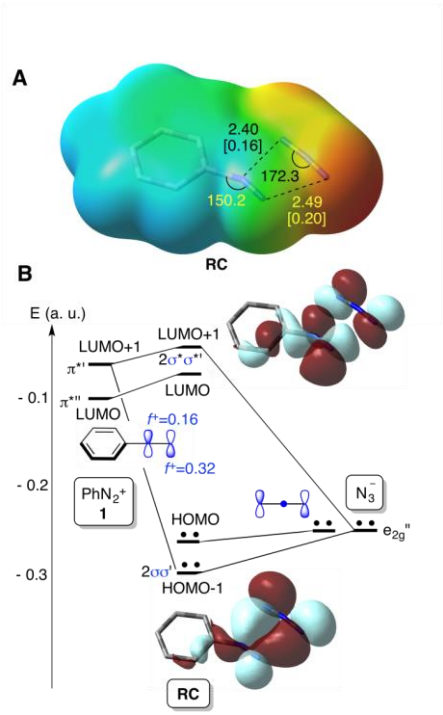

Figure 1. (A) Electrostaic potential and chief geometric features of complex **RC** associated with the interaction between azide anion and diazonium cation **1**. Bond distances and angles are given in Å and deg., respectively. Numbers in square brackets are the corresponding bond indices. (B) Selected Kohn-Sham molecular orbitals of **RC**. Descriptors f^+ on the nitrogen atoms correspond to the local Fukui indices.

In view of these results, we performed DFT[18] calculations on the parent PhN_2^+(**1**)+N_3^- → PhN_3(**2**)+N_2 reaction in order to obtain evidences about the most plausible reaction mechanism and get a better understanding of the experimental data. A M06-2X[19] (PCM)[20]/def2-TZVPP[21] study of the reactants in aqueous solution revealed the presence of a local minimum associated with a weak complex formed denoted as **RC** in Figure 1.

This stationary point on the potential energy surface (PES) consists of a charge transfer complex, in which both ionic reactants are in close contact, with a calculated charge transfer of 0.5 a.u. The new N-N bond distances are ca. 2.4-2.5 Å (Figure 1A), the respective Wiberg bond indices[22] being of ca. 0.2. This weak

bonding pattern stems form a two-electron interaction between one of the e_{2g}" MO's of the azide anion and the in-plane π*' LUMO+1 of **1** (Figure 1B). The occupied MO's π" □of **1** and e_{1g} of N_3^- lead to a destabilizing four-electron interaction (not shown), thus resulting in a very weak bonding pattern between both reactants at **RC**. Actually, this stationary point is not stabilized with respect to the separate reactants at 298 K (Figure 2).

From these reactants we characterized saddle point **TS$_{SN2}$** (Figure 2) with computed activation energy of ca. 27 kcal/mol. The geometric features of this transition structure are quite similar to those obtained for solvolysis reactions of aromatic diazonium salts.[11] In our case, however, there is an additional interaction between the diazonium and azide moieties (Figure 1). This remarkable barrier and our experimental results permit to discard the S_N2Ar mechanism for this particular reaction.

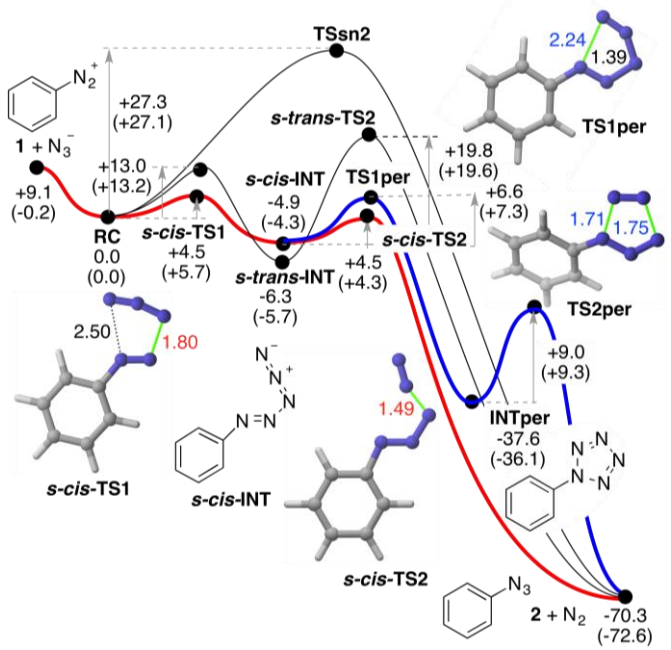

Figure 2. M06-2X(PCM)/def2-TZVPP reaction profiles associated with the reaction between diazonium cation **1** and azide anion to yield phenyl azide **2** and dinitrogen. Numbers close to reactants, intermediates and products indicate the relative energies in kcal/mol. Numbers close to the arrows indicate the respective activation energies, in kcal/mol. Numbers in parentheses indicate the respective Gibbs energies, computed at 298 K, in kcal/mol. The lowest energy reaction paths are highlighted in red and yellow.

The frontier MO's of the reactants at **RC** are also indicated in Figure 1B and correspond to in-plane □-MO's e_{2g}" and π*". These computational data are compatible with a high electrophilicity associated with the terminal nitrogen of the diazonium moiety of **1**, with a local electrophilic Fukui index[23] f^+ of 0.32 a.u. (Figure 1B). The interaction between the terminal nitrogen atoms of both reactants according to the mechanism reported in eq. (3) lead to saddle points ***s-cis***- and ***s-trans*-TS1** (Figure 2). The former transition structure was calculated to be ca. 7 kcal/mol less energetic than the latter (Figure 2). The chief geometric features of ***s-cis*-TS1** closely resemble those expected for an asynchronous transition structure associated with a (3+2) cycloaddition.[24] However, all our attempts to connect directly ***s-cis*-TS1** with 2-phenyl-2*H*-pentazole **INTper** were unfruitful. Instead, this saddle point led to zwitterionic intermediate ***s-cis*-INT**, from which we located transition structure **TS1per**. This latter saddle point led to 2-phenyl-2*H*-pentazole **INTper** (Figure 2), associated with this hypothetical (3+2) cycloaddition. From this local minimum we found saddle point **TS2per** leading to phenyl azide **2**. Although this latter transition structure associated with a retro-(3+2) cycloaddition is compatible with the reaction scheme gathered in eq. (2), it is important to note that **INTper** does not stem from **RC** but from ***s-cis*-INT**, which constitutes the key intermediate of the less energetic reaction profiles. In addition, our calculations indicate that formation of **INTper** occurs with an activation barrier that is ca. 2 kcal/mol higher than that associated with formation of phenyl azide **2**.

Intrinsic Reaction coordinate[25] (IRC) scans from both ***s-cis***- and ***s-trans*-TS1** led to the corresponding zwitterionic intermediates ***s-cis***- and ***s-trans*-INT** (see Electronic Supporting Information). The relative stabilities of these polar intermediates were found to be the opposite ones with respect to the corresponding transition structures. Therefore, the preferred route to yield azidobenzene **2** and dinitrogen occurs via ***s-cis*-TS2** in which the cleavage of the PhN_3(-)-N_2(+) delocalized bond is produced (Figure 2). This low barrier is associated with the formation of dinitrogen and azidobenzene **2**, two neutral stabilized species.

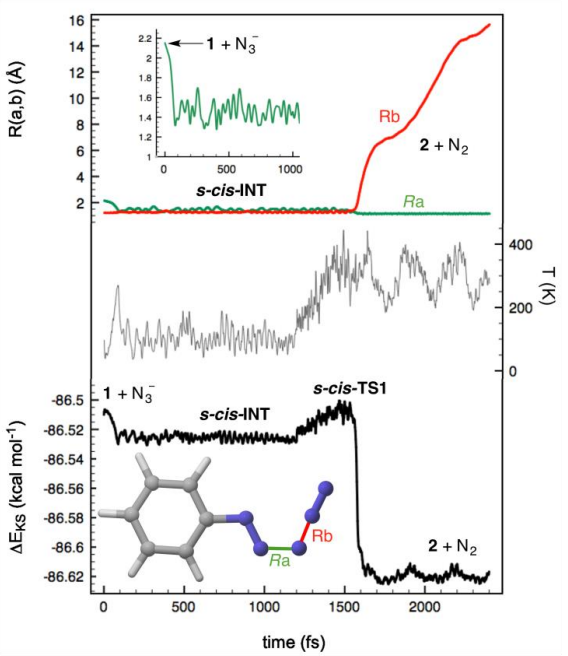

Figure 3. Car-Parrinello Molecular Dynamics (CPMD) plots of the reaction between diazonium cation **1** and azide anion to yield phenyl azide **2** and dinitrogen.

In order to confirm the preference for the mechanism outlined in eq. (3) we carried out Car-Parrinello[26] Molecular Dynamics (CPMD)[27] within the DFT framework, using the BLYP gradient-corrected functional[28] and ultrasoft Vanderbilt pseudopotentials.[29] These simulations were carried out at different temperatures with a 1 fs time step for integration of equations of motion. Our CPMD results for the entire PhN_2^+(**1**)+N_3^- → PhN_3(**2**)+N_2 reaction confirmed that the reactants at internuclear distances similar to those found in complex **RC** form ***s-cis*-INT** zwitterion in less than 100 fs at 100 K (Figure 3). This intermediate is stable at this temperature within a time span of at least 1.2 ns. When the system was heated at ca. 300 K, the system reached ***s-cis*-TS2** in ca. 300 fs to yield the reaction products,[30] thus confirming the stepwise nature of the reaction via open intermediates of type **INT**. These results are in agreement with our experimental results and provide a rationale for

the loss of radioactivity observed when radiolabelled azide anion was used following method A (Scheme 1).

Kinetic simulations carried out using reaction paths highlighted in red and blue in Figure 2 indicate that ca. 99 % of **2** stems from ***s-cis*-TS2**, whereas ca. 1 % of the reaction product is formed via **INTper** (see the Electronic Supplementary Information for additional details). These results are in good agreement with the release of $[^{13}N]N_2$ obtained in our experimental studies following synthetic strategy shown in Scheme 1, method A.

In conclusion, we have demonstrated using experimental and computational data that the formation of aryl azides from the corresponding diazonium salts occurs via a stepwise mechanism via acyclic zwitterionic intermediates. The use of the short-lived positron emitter nitrogen-13 for the elucidation of reaction mechanisms is unprecedented; hence, the work here reported can inspire future applications of this radionuclide beyond the preparation of radiolabelled compounds for imaging studies.

We acknowledge financial support from RADIOMI project (EU FP7-PEOPLE-2012-ITN-RADIOMI), the Ministerio de Economía y Competitividad (MINECO) of Spain and FEDER (project CTQ2013-45415-P), the University of the Basque Country (UPV/EHU, UFI11/22 QOSYC), and the Basque Government (GV/EJ, grant IT-324-07). A. de C. and F. P. C. thank the SGI/IZO-SGIker (UPV/EHU) and the DIPC for generous allocation of computational resources.

Notes and references

[a] Radiochemistry and Nuclear Imaging, CIC biomaGUNE, Paseo Miramón 182, Parque Tecnológico de San Sebastián, 20009 San Sebastián/Donostia, Spain.

[b] Departamento de Química Orgánica I, Facultad de Química, Universidad del País Vasco/Euskal Herriko Unibertsitatea (UPV/EHU), 20018 San Sebastián/Donostia, Spain.

[c] Ikerbasque, Basque Foundation for Science, 48018, Bilbao, Spain.

[d] Centro de Innovación en Química Avanzada (ORFEO-CINQA).

[e] Donostia International Physics Center (DIPC), 20018, San Sebastián/Donostia, Spain.

[f] Radiochemistry Platform, CIC biomaGUNE, Paseo Miramón 182, Parque Tecnológico de San Sebastián, 20009, San Sebastián/Donostia, Spain.

[g] Department of Radiation Physics and Department of Medical and Health Sciences, Linköping University, Linköping, Sweden.

*E-mail: Jordi Llop (jllop@cicbiomagune.es, chemical synthesis and radiochemistry), Fernando P. Cossío (fp.cossio@ehu.es, computational studies).

† Electronic Supplementary Information (ESI) available: Experimental procedures for the synthesis of ^{13}N-labeled phenyl azide, and identification of the labeled species by radio-HPLC and GC-MS. Energies, zero-point vibrational energies, Gibbs energy corrections and Cartesian coordinates of all the stationary points discussed in this work. Movie including the CPMD simulations. Full ref. 18. See DOI: 10.1039/c000000x/

1 (a) P. Grieß, *Philos. Trans. R. Soc. London*, 1864, **13**, 377. (b) P. Grieß, *Justus Liebigs Ann. Chem.*, 1865, **135**, 131.
2 (a) Y. S. Klausner, M. Bodanshky, *Synthesis*, 1974, 549-559; (b) S.-Y. Han, Y.-A. Kim, *Tetrahedron*, 2004, **60**, 2447-2467.
3 T. S. Lin, W. H. T. Prusoff, *J. Med. Chem.*, 1978, **21**, 109-112.
4 H. M. S. Kumar, B. V. S. Reddy, S. Anjaneyulu, J. S. Yadav, *Tetrahedron Lett.*, 1999, **40**, 8305-8306.
5 G. C. Tron, T. Pirali, R. A. Billington, P. L. Canonico, G. Sorba, A. A. Genazzani, *Med. Res. Rev.*, 2008, **28**, 278-308.
6 C. I. Schilling, N. Jung, M. Biskup, U. Schepers, S. Bräse, *Chem. Soc. Rev.*, 2011, **40**, 4840-4871.
7 (a) S. X. Cai, D. J. Glenn, K. R. Gee, M. D. Yan, R. E. Cotter, N. L. Reddy, E. Weber, J. F. W. Keana, *Bioconjugate Chem.*, 1993, **4**, 545-548; (b) S. X. Cai, D. J. Glenn, M. Kanskar, M. Wybourne, N. J. F. W. Keana, *Chem. Mater.*, 1994, **6**, 1822-1829; (c) E. W. Meijer, S. Nijhuis, F. C. B. M. Van Vroonhoven, *J. Am. Chem. Soc.*, 1988, **110**, 7209-7210.
8 (a) E. Noelting, O. Michel, *Ber. Dtsch. Chem. Ges.*, 1893, **26**, 86-87; (b) E. Noelting, O. Michel, *Ber. Dtsch. Chem. Ges.*, 1893, **26**, 88-92.
9 E. Noelting, E. Grandmougin, O. Michel, *Ber. Dtsch. Chem. Ges.*, 1892, **25**, 3328-3342.
10 (a) J. C. Kauer, R. A. Carboni, *J. Am. Chem. Soc.*, 1967, **89**, 2633-2637; (b) M. Takahashi, D. Suga, *Synthesis*, 1998, **7**, 986-990.
11 (a) A. García-Martínez, S. de la Moya-Cerero, J. Osío-Barcina, F. Moreno-Jiménez, B. Lora-Maroto, *Eur. J. Org. Chem.*, 2013, 6098-6107. (b) B. R. Ussing, D. A. Singleton, *J. Am. Chem. Soc.*, 2005, **127**, 2888-2899. (c) Z. Wu, R. Glaser, *J. Am. Chem. Soc.*, 2004, **126**, 10632-10639. (d) I. M. Cuccovia, M. A. da Silva, H. M. C. Ferraz, Jr., J. R. Pliego, J. M. Riveros, H. J. Chaimovich, *Chem. Soc., Perkin Trans. 2*, 2000, 1896-1907.
12 For analogous (3+2) cycloadditions involving arsa-diazonium salts see: M. Kuprat, A. Schultz, A. Villinger, *Angew. Chem. Int. Ed.*, 2013, **52**, 7126-7130.
13 R. N. Butler, A. Fox, S. Collier, L. A. Burke, *J. Chem. Soc. Perkin Trans. 2*, 1998, 2243-2247.
14 V. Gómez-Vallejo, K. Kato, M. Hanyu, K. Minegishi, J. I. Borrell, J. Llop, *Bioorg. Med. Chem. Lett.*, 2009, **19**, 1913.
15 (a) J. Llop, V. Gómez-Vallejo, M. Bosque, G. Quincoces, I. Peñuelas, *Appl. Radiat. Isotopes*, 2009, **67**, 95. (b) V. Gómez-Vallejo, K. Kato, I. Oliden, J. Calvo, Z. Baz, J. I. Borrell, J. Llop, *Tetrahedron Lett.*, 2010, **51**, 2990.
16 (a) V. Gomez-Vallejo, J. I. Borrell, J. Llop, *Eur. J. Med. Chem.*, 2010, **45**, 5318. (b) V. Gaja, V. Gomez-Vallejo, M. Puigivila, C. Perez-Campana, A. Martin, A. Garcia-Osta, T. Calvo-Fernandez, M. Cuadrado-Tejedor, R. Franco, J. Llop, *Mol. Imaging Biol.*, 2014, **16**, 5380.
17 A. A. Siddiki, B. S. Takale, V. N. Telvekar, *Tetrahedron Lett.*, 2013, **54**, 1294-1297.
18 Gaussian 09, Revision B.1., M. J. Frisch, et al., Gaussian, Inc., Wallingford CT, 2009.
19 (a) Y. Zhao, D. G. Truhlar, *Acc. Chem. Res.*, 2008, **41**, 157-167. (b) Y. Zhao, D. G. Truhlar, *Theor. Chem. Acc.*, 2008, **120**, 215-241.
20 (a) S. Miertuš, E. Scrocco, J. Tomasi, *Chem. Phys.*, 1981, **55**, 117-129. (b) J. Tomasi, B. Mennucci, R. Cammi, *Chem. Rev.*, 2005, **105**, 2999-3093.
21 F. Weigend, R. Ahirichs, *Phys. Chem. Chem. Phys.*, 2005, **7**, 3297-3305.
22 K. Wiberg, *Tetrahedron*, 1968, **24**, 1083-1096.
23 (a) K. Fukui, *Acc. Chem. Res.*, 1981, **14**, 363-368. (b) P. W. Ayers, W. Yang, L. J. Bartolotti, The Fukui Function. In Chemical Reactivity Theory: A Density Functional View. Chattaraj, P., Ed.; Taylor & Francis: Boca Ratón, 2009; pp 255- 267 and references therein.
24 (a) A. de Cózar, F. P. Cossío, *Phys. Chem. Chem. Phys.*, 2011, **13**, 10858-10868. (b) I. Fernández, F. P. Cossío, F. M. Bickelhaupt, *J. Org. Chem.*, 2011, **76**, 2310-2314.
25 C. González, H. B. Schlegel, *J. Phys. Chem.*, 1990, **94**, 5523-5527.
26 R. Car, M. Parrinello, *Phys. Rev. Lett.*, 1985, **55**, 2471-2474.
27 CPMD code (http://www.cpmd.org): Copyright MPI für Festkçrperforschung, Stuttgart, and IBM Zürich Research Laboratory, 1990–2006.
28 (a) A. D. Becke, *Phys. Rev. A*, 1988, **38**, 3098–3100. (b) C. Lee, W. Yang, R. C. Parr, *Phys. Rev. B*, 1988, **37**, 785–789.
29 D. Vanderbilt, *Phys. Rev. B*, 1990, **41**, 7892–7895.
30 See movie SM1 in the Electronic Supplementary Information.

Supporting Information

Synthesis of Radiolabelled Aryl Azides from Diazonium Salts: Experimental and Computational Results Permit to Select the Preferred Mechanism

Sameer M. Joshi,[a] Abel de Cózar,[b,c,d,e] Vanessa Gómez-Vallejo,[f] Jacek Koziorowski,[g] Jordi Llop,[a,] and Fernando P. Cossío[b,d,e*.]*

jllop@cicbiomagune.es, fp.cossio@ehu.es

[a] *Radiochemistry and Nuclear Imaging, CIC biomaGUNE, Paseo Miramón 182, Parque Tecnológico de San Sebastián, 20009 San Sebastián/Donostia, Spain.*
[b] *Departamento de Química Orgánica I, Facultad de Química, Universidad del País Vasco/Euskal Herriko Unibertsitatea (UPV/EHU), 20018 San Sebastián/Donostia, Spain.*
[c] *Ikerbasque, Basque Foundation for Science, 48018, Bilbao, Spain.*
[d] *Centro de Innovación en Química Avanzada (ORFEO-CINQA).*
[e] *Donostia International Physics Center (DIPC), 20018, San Sebastián/Donostia, Spain.*
[f] *Radiochemistry Platform, CIC biomaGUNE, Paseo Miramón 182, Parque Tecnológico de San Sebastián, 20009, San Sebastián/Donostia, Spain.*
[g] *Department of Radiation Physics and Department of Medical and Health Sciences, Linköping University, Linköping, Sweden.*

CONTENTS

General Information

Aniline (reagent plus grade 99%), sodium nitrite (ACS reagent, 97%), acetic acid (Reagentplus®, >99%), hydrazine hydrate solution (iodometric, 78-82%), and azidobenzene solution (0.5 M in tert-butyl methyl ether, >95%) were purchased from Sigma-Aldrich and used without further purification. Hydrochloric acid (37%, extrapure, Ph. Eur.) and dichloromethane (synthesis grade) were purchased from Scharlau. Ultrapure water (Type I water, ISO 3696) was obtained from a Milli-Q® system (Merck Millipore).

Synthesis of ^{13}N-labelled phenylazide (Route B in Scheme 1)

Nitrogen-13 (30 mCi, 1110 GBq) was produced in an IBA Cyclone 18/9 cyclotron by irradiation of purified water *via* the $^{16}O(p,\alpha)^{13}N$ nuclear reaction. The irradiated solution was passed through a glass column filled with pre-treated cadmium[1] to quantitatively reduce $[^{13}N]NO_3^-$ into $[^{13}N]NO_2^-$. A sample of this solution (20 µL) was analyzed by HPLC to confirm quantitative reduction of $[^{13}N]NO_3^-$ into $[^{13}N]NO_2^-$, using an Agilent 1200 series HPLC equipped with a quaternary pump, a multiple wavelength detector and a radiometric detector (Gabi, Raytest). An HP Asahipak ODP-50 (5 µm, 125x4 mm, Teknokroma, Spain) was used as stationary phase, and a solution containing additive for ionic chromatography (15 mL) in a mixture water/acetonitrile (86/14, V = 1L) basified to pH = 8.6 with 1M sodium hydroxide solution was used as the mobile phase at a flow rate of 1 mL/min. Simultaneous UV (λ = 254 nm) and isotopic detection were used.

The solution containing $[^{13}N]NO_2^-$ was added drop-wise to a second solution containing aniline (23mg, 0.25 mmole) in HCl (0.1mL of 37% HCl in 0.15mL water). The reaction for the formation of the diazonium salt was allowed to occur (1 minute, RT). In a separate vial, a mixture of sodium nitrite solution (17mg in 0.1mL water, 0.25 mmole), acetic acid (120 µL, 1.98 mmole) and hydrazine hydrate solution (70 µL, 1.41 mmole) was prepared and added drop-wise to the previous solution (total addition time 1 min, and the reaction for the formation of ^{13}N-labelled azide was allowed to occur for 1 min. The activity (A_1) was measured in a dose calibrator (PETDOSE HC, Comecer), the vial was flushed with nitrogen gas (1 minute) and the activity was measured again (A_2). The amount of $[^{13}N]N_2$ was calculated as A_2-A_1. The reaction crude was analyzed by HPLC using an Agilent 1200 Series HPLC system with a multiple wavelength UV detector (λ = 254 nm) and a radiometric detector (Gabi, Raytest). A RP-C18 column (Mediterranean Sea18, 4.6x250 mm, 5 µm particle size) was used as stationary phase and ammonium formate (pH = 3.9) (A)/methanol (B) was used as the mobile phase. The following gradient was used: t=0 min, 90%A/10%B; t=2 min, 90%A/10%B; t=4 min, 35%A/65%B; t=6 min, 20%A/80%B; t=12 min, 20%A/80%B; t=15 min, 90%A/10%B. The presence of the desired labelled specie was confirmed by co-elution with reference

[1] Cadmium (20 g., granular, 5-20 mesh) was introduced in a glass column (10 mm i.d., 8 cm in length) and sequentially washed with 1 M HCl (2 x 20 mL), distilled water (3 x 20 mL), 0.5 M aqueous $CuSO_4$ solution (2 x 20 mL), 0.1 M aqueous NH_4Cl solution (2 x 20 mL) and distilled water (3 x 20 mL).

standard (retention time = 9.6 min, see Figure S1). The amount of [^{13}N]phenylazide was determined as the product (A_2 x A_U), where A_U is the area under the peak for phenyl azide (radiometric detector, expressed as percentage with respect to all integrated peaks in the chromatogram). All radioactivity values were decay corrected to the same time point.

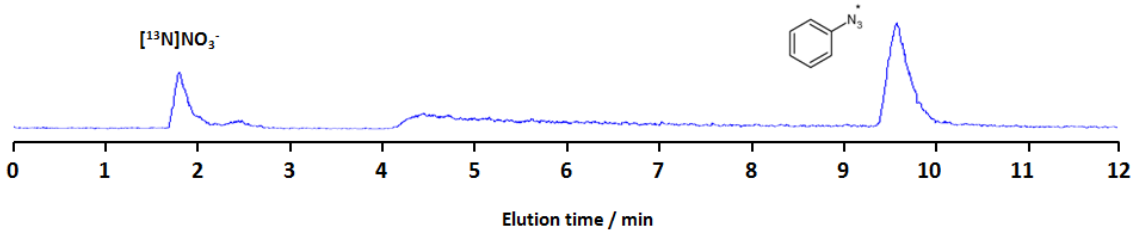

Figure S1: HPLC Chromatographic profile of the reaction mixture. The labelled azide appears at t=9.6 min.

Synthesis of ^{13}N-labelled phenylazide (Route A in Scheme 1)

[^{13}N]NO_2^- was prepared as mentioned in route B. The resulting solution was added drop-wise to a solution containing hydrazine hydrate solution (70 µL, 1.41 mmole) and acetic acid (120 µL, 1.98 mmole), and the reaction was allowed to occur (1 minute, RT). In a separate vial, a solution of aniline (23mg, 0.25 mmole) in HCl (0.1mL of 37% HCl in 0.15mL water) was reacted with sodium nitrite (17mg in 0.1mL water, 0.25 mmole) for 1 minute at RT to form the non-radioactive diazonium salt. The first solution was added drop wise to the second solution (total duration 1 minute) and the reaction was allowed to occur (1 min, RT). Sample processing, identification of the labelled species and determination of the amount of [^{13}N]N_2 and [^{13}N]phenyl azide was performed as in Route B.

Analysis of the radioactive gas

The synthesis of ^{13}N-labelled phenylazide was performed following the methodologies described above. However, before flushing the reaction vials with nitrogen gas, a sample of the gas from the sealed reaction vial was withdrawn and analyzed by radio-GC-MS. Analyses were performed on an Agilent 7820A network GC with an automatic loop injection system (loop volume = 250 µL) combined with an Agilent 5975c inert XL MSD with Triple axis detector. A J&W PoraPLOT column (length 27.5m, internal diameter 0.32 mm) was used as stationary phase. The inlet conditions were 150 °C, 25 psi and a flow rate of 3.5 mL/min using a 1:10 split injector with helium (99.9999%) as the carrier gas. The oven temperature was set to 36 °C. Total run time was 6 min (retention time = 1.45 min). Simultaneous detection using a radiometric detector (Gabi, raytest) and MS were used using a post-column split. MS was operated in scan mode in the range 10-150 Da.

Computational Results

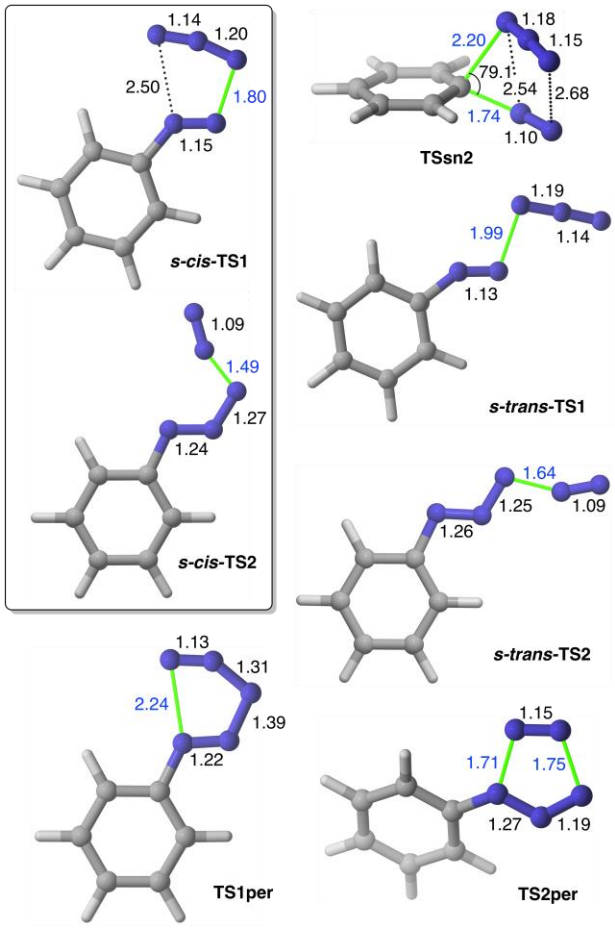

Figure S2. Chief geometric features (M06-2X/def2-TZVPP level of theory) of transition structures gathered in Figure 2 of the main text. Bond distances and angles are given in Å and deg., respectively.

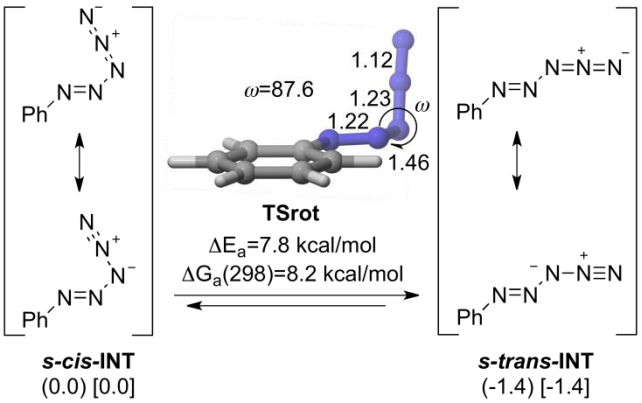

Figure S3. M06-2X(PCM)/def2-TXVPP relative energies (in kcal/mol, numbers in parentheses) and relative Gibbs energies (at 298 K, in kcal/mol, numbers in square brackets) of zwitterionic intermediates ***s-cis***- and ***s-trans*-INT**. The main geometric features and activation energies of transition structure **TSrot** that connects both conformers are also indicated. Bond distances and angles are given in Å and deg., respectively. Dihedral angle ω describes the torsion about the N2-N3 bond.

Kinetic Simulations

Since the ensemble of alternative reaction paths gives rise to a complex mechanistic scheme, we performed numeric kinetic simulations in order to evaluate the impact of each possible mechanism on the formation of phenylazide **2** at 298 K. First, we computed the kinetic constants associated with each elementary step from the corresponding free energy values reported in Table S1 according to the Eyring equation ($k_i=(k_bT/h)\exp[-\Delta G_a/RT]$). These values are gathered in Table S2. The notation used for the different kinetic constants is that indicated in Figure S4.

Table S1. Total electronic energies[a] (E, in a.u.), zero point correction of energy[b] (ZPCE, in a.u.), thermal corrections to Gibbs free energies[b] (TCGE, in a. u.) and number of imaginary frequencies[c] (NIMAG) of all stationary points discussed in the main text.

Structure	E	ZPCE	TCGE	NIMAG(ν)
1	-340.909241	0.100227	0.069959	0
N_3^-	-164.331227	0.011302	-0.009852	0
RC	-505.256076	0.112680	0.076092	0
***s-cis*-INT1**	-505.264761	0.113499	0.077939	0
***s-trans*-INT1**	-505.267179	0.113810	0.078329	0
INTper	-505.320504	0.117115	0.082928	0
2+N_2	-505. 666837	0.111213	0.070915	0
2	-395.829422	0.104537	0.072625	0
N_2	-109.536273	0.005741	-0.012675	0
***s-cis*-TS1**	-505.248494	0.112217	0.077531	1 (-171.8042)
***s-trans*-TS1**	-505. 234044	0.111455	0.075186	1 (-235.5360)
***s-cis*-TS2**	-505.255313	0.111201	0.075298	1 (-752.6364)
***s-trans*-TS2**	-505.231858	0.110073	0.074182	1 (-708.9640)
TSrot	-505.252342	0.113447	0.078639	1 (-152.8671)
TSsn2	-505.216889	0.109043	0.073751	1 (-554.9892)
TS1per	-505.253207	0.112444	0.078048	1 (-323.7562)
TS2per	-505.272447	0.112528	0.078006	1 (-646.9926)

[a]Computed at the M06-2X(PCM)/def2-TZVPP level of theory. [b]Computed at 298 K at the M06-2X(PCM)/def2-TZVPP level of theory. [c]When NIMAG=1, the imaginary frequency ν (in parentheses) is given in cm^{-1}.

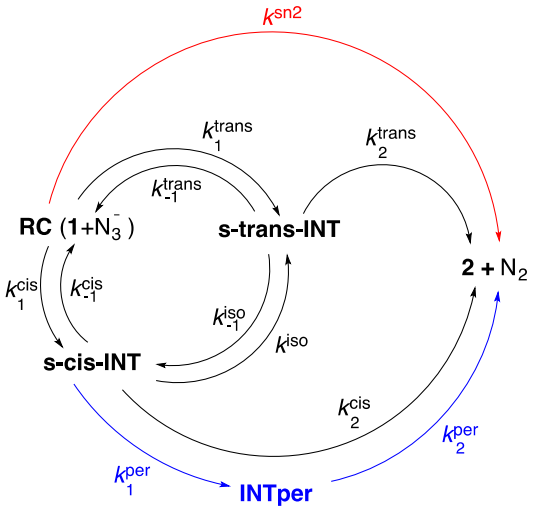

Figure S4. Kinetic scheme and kinetic rate constants associated with the elementary steps corresponding to the **1**+N_3^- → **2**+N_2 reaction.

Table S2. Calculated kinetic constants[a] (k_i^a, s^{-1}) associated with the formation of **2** computed using Eyring equation and the corresponding Gibbs free energy barriers.

Elementary step	k_i^a	Value
RC (**1**+N_3^-) → **2**+N_2	k^{sn2}	8.4 x 10^{-8}
RC (**1**+N_3^-) → *s-trans*-**INT**	k_1^{trans}	1.3 x 10^{3}
s-trans-**INT** → **RC** (**1**+N_3^-)	k_{-1}^{trans}	8.6 x 10^{-2}
RC (**1**+N_3^-) → *s-cis*-**INT**	k_1^{cis}	4.1 x 10^{8}
s-cis-**INT** → **RC** (**1**+N_3^-)	k_{-1}^{cis}	2.9 x 10^{5}
s-trans-**INT** → **2**+N_2	k_2^{trans}	2.6 x 10^{-2}
s-cis-**INT** → **2**+N_2	k_2^{cis}	4.3 x 10^{9}
s-cis-**INT** → **INT**per	k_1^{per}	2.7 x 10^{7}
INTper → **2**+N_2	k_2^{per}	9.4 x 10^{5}
s-cis-**INT** → *s-trans*-**INT**	k^{iso}	6.6 x 10^{6}
s-trans-**INT** → *s-cis*-**INT**	k_{-1}^{iso}	6.3 x 10^{7}

[a]Values computed at 298.15 K.

According to the kinetic scheme gathered in Figures 2 and S4, formation of **2** from the corresponding reaction intermediates can be assumed as irreversible and therefore the total reaction rate can be described by the following equation:

$$rate = k^{sn2}[RC] + k_2^{cis}[scisINT] + k_2^{trans}[stransINT] + k_2^{per}[INTper] \quad (1)$$

The evolution of the different reaction intermediates can be described as indicated in equations (2)-(5):

$$\frac{d}{dt}[RC] = -\left(k^{sn2} + k_1^{cis} + k_1^{trans}\right)[RC] + k_{-1}^{cis}[scisINT] + k_{-1}^{trans}[stransINT] \quad (2)$$

$$\frac{d}{dt}[scisINT] = k_1^{cis}[RC] + k_{-1}^{iso}[stransINT] - \left(k_{-1}^{cis} + k^{iso} + k_1^{per} + k_2^{cis}\right)[scisINT] \quad (3)$$

$$\frac{d}{dt}[stransINT] = k_1^{trans}[RC] + k^{iso}[scisINT] - \left(k_{-1}^{cis} + k_{-1}^{iso} + k_2^{trans}\right)[stransINT] \quad (4)$$

$$\frac{d}{dt}[INTper] = k_1^{per}[scisINT] - k_2^{per}[INTper] \quad (5)$$

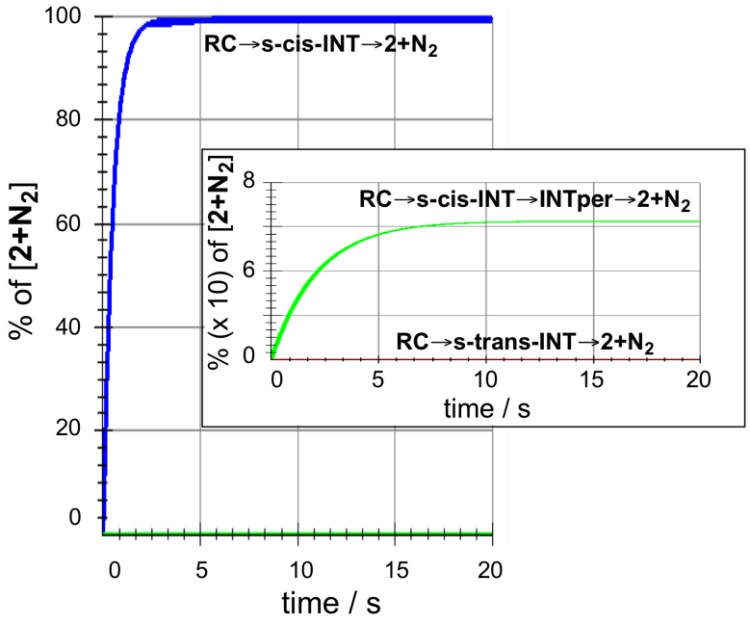

Figure S5. Simulated reaction outcome obtained by numerical integration of the previous kinetic equations using eqs. (1-n) and the rate constants collected in Table S2. The inset highlights the formation of **2** via **INTper**.

Numerical integration of equations (1)-(5) showed the quick stabilization of products **2**+N_2, as it is shown in Figure S5. Using these results, we were able to identify the contribution of the different reaction paths to the formation of phenylazide. As it can be seen by inspection of Figure S5, nearly all the reaction products **2** and N_2 stem from zwitterionic intermediate ***s-cis*-INT**. A careful analysis revealed the low but measurable contribution of five-membered intermediate **INTper** to the final outcome, which can be estimated as $0.72 \gg 1$ %, the contribution of zwitterionic route via ***s-cis*-INT** being therefore of ca. 99 %. Neither the direct S_N2 reaction nor the stepwise process via ***s-trans*-INT** (including the isomerization reaction) contributed significantly to the formation of reaction product **2**.

Cartesian coordinates (optimized at the M06-2X(PCM)/def2-TZVPP level) of all the stationary points discussed in the main text.

1

Center Number	Atomic Number	Atomic Type	Coordinates (Angstroms) X	Y	Z
1	6	0	0.547198	0.001774	0.001999
2	7	0	1.941521	0.000945	0.000148
3	6	0	-0.095581	1.235927	0.001920
4	6	0	-1.476229	1.212972	-0.000148
5	6	0	-2.155036	-0.001939	-0.002292
6	6	0	-1.473155	-1.215022	-0.000158
7	6	0	-0.092597	-1.233718	0.001943
8	7	0	3.030743	-0.000498	-0.002954
9	1	0	0.468220	2.156527	0.003431
10	1	0	-2.023186	2.143974	-0.000638
11	1	0	-3.235936	-0.003507	-0.005542
12	1	0	-2.017010	-2.147821	-0.000708
13	1	0	0.474462	-2.152263	0.003512

N_3^-

Center Number	Atomic Number	Atomic Type	Coordinates (Angstroms) X	Y	Z
1	7	0	0.000000	0.000000	0.000000
2	7	0	0.000000	0.000000	-1.167881
3	7	0	0.000000	0.000000	1.167881

RC

Center Number	Atomic Number	Atomic Type	Coordinates (Angstroms) X	Y	Z
1	6	0	0.541538	-0.265922	0.037324
2	7	0	-0.818474	-0.690728	0.080948
3	6	0	0.864591	1.076521	0.111707
4	6	0	2.209311	1.408857	0.079031
5	6	0	3.176004	0.417511	-0.031613
6	7	0	-1.571815	-1.501090	0.144431
7	7	0	-3.734721	-0.260247	-0.008356
8	6	0	2.815686	-0.923975	-0.106443
9	6	0	1.482519	-1.286377	-0.068638
10	7	0	-2.960817	0.599016	-0.082911
11	7	0	-2.069121	1.352753	-0.145637

12	1	0	0.082129	1.813369	0.190541
13	1	0	2.499870	2.447758	0.137514
14	1	0	4.221815	0.690798	-0.060192
15	1	0	3.572202	-1.690336	-0.194273
16	1	0	1.170738	-2.319205	-0.121115

s-cis-INT1

Center Number	Atomic Number	Atomic Type	Coordinates (Angstroms) X	Y	Z
1	6	0	0.000000	0.598394	0.000000
2	7	0	0.112464	-0.820642	0.000000
3	6	0	1.205480	1.289145	0.000000
4	6	0	1.207441	2.677025	0.000000
5	6	0	0.005321	3.369584	0.000000
6	7	0	-0.955702	-1.431123	0.000000
7	7	0	-0.857250	-2.821287	0.000000
8	6	0	-1.200476	2.672885	0.000000
9	6	0	-1.211696	1.289038	0.000000
10	7	0	0.337828	-3.228361	0.000000
11	7	0	1.357841	-3.659571	0.000000
12	1	0	2.129113	0.726201	0.000000
13	1	0	2.145783	3.214304	0.000000
14	1	0	0.003126	4.451037	0.000000
15	1	0	-2.136434	3.214880	0.000000
16	1	0	-2.144281	0.744046	0.000000

s-trans-INT1

Center Number	Atomic Number	Atomic Type	Coordinates (Angstroms) X	Y	Z
1	6	0	0.000000	0.856678	0.000000
2	7	0	-1.030652	-0.126277	0.000000
3	6	0	-0.438793	2.175205	0.000000
4	6	0	0.483344	3.212393	0.000000
5	6	0	1.841808	2.929772	0.000000
6	7	0	-0.627409	-1.287065	0.000000
7	7	0	-1.708876	-2.166999	0.000000
8	6	0	2.277887	1.607173	0.000000
9	6	0	1.365133	0.567395	0.000000
10	7	0	-1.267724	-3.340966	0.000000
11	7	0	-0.995849	-4.416461	0.000000
12	1	0	-1.502726	2.370109	0.000000
13	1	0	0.139853	4.237732	0.000000
14	1	0	2.562857	3.735919	0.000000
15	1	0	3.337154	1.388472	0.000000
16	1	0	1.700150	-0.459550	0.000000

INTper

Center Number	Atomic Number	Atomic Type	Coordinates (Angstroms) X	Y	Z
1	6	0	-0.386335	0.000002	0.000004
2	7	0	1.044196	-0.000005	0.000006
3	6	0	-1.054887	-1.214102	0.000527
4	6	0	-2.441072	-1.203234	0.000510
5	6	0	-3.134373	0.000000	0.000001
6	7	0	1.782453	1.082314	0.001142
7	7	0	2.999270	0.665263	0.000622
8	6	0	-2.441069	1.203233	-0.000506
9	6	0	-1.054883	1.214107	-0.000523
10	7	0	2.999261	-0.665258	-0.000588
11	7	0	1.782450	-1.082322	-0.001193
12	1	0	-0.502885	-2.141942	0.000987
13	1	0	-2.978238	-2.141195	0.000963
14	1	0	-4.215441	0.000006	-0.000002
15	1	0	-2.978236	2.141195	-0.000965
16	1	0	-0.502890	2.141952	-0.000980

2+N_2

Center Number	Atomic Number	Atomic Type	Coordinates (Angstroms) X	Y	Z
1	6	0	0.497408	-0.164416	-0.487241
2	7	0	-0.771697	-0.312123	-1.111936
3	6	0	1.365426	0.752078	-1.072997
4	6	0	2.622966	0.950123	-0.525505
5	6	0	3.020599	0.240300	0.602147
6	7	0	-1.549117	-1.106331	-0.587054
7	7	0	-2.323969	-1.798777	-0.178073
8	6	0	2.147675	-0.670994	1.181288
9	6	0	0.885037	-0.878263	0.643428
10	7	0	-3.344007	1.130310	0.916438
11	7	0	-2.616529	1.814269	0.489054
12	1	0	1.043721	1.296952	-1.950413
13	1	0	3.295676	1.662883	-0.983630
14	1	0	4.003188	0.396073	1.025938
15	1	0	2.446991	-1.228451	2.059073
16	1	0	0.212995	-1.591853	1.103307

2

Center Number	Atomic Number	Atomic Type	Coordinates (Angstroms) X	Y	Z
1	6	0	0.152349	-0.376347	0.000338
2	7	0	1.469412	-0.910821	0.000555
3	6	0	-0.126474	0.987524	0.000430
4	6	0	-1.447315	1.413272	0.000102
5	6	0	-2.486359	0.492618	-0.000276
6	6	0	-2.197422	-0.867401	-0.000303
7	6	0	-0.883361	-1.305576	0.000019
8	7	0	3.292619	0.561229	-0.000604
9	7	0	2.391348	-0.097679	-0.000181
10	1	0	0.676228	1.713886	0.000846
11	1	0	-1.661003	2.473648	0.000145
12	1	0	-3.512963	0.831692	-0.000549
13	1	0	-3.000030	-1.592576	-0.000607
14	1	0	-0.644405	-2.360286	-0.000085

N_2

Center Number	Atomic Number	Atomic Type	Coordinates (Angstroms) X	Y	Z
1	7	0	0.000000	0.000000	0.542886
2	7	0	0.000000	0.000000	-0.542886

***s-cis*-TS1**

Center Number	Atomic Number	Atomic Type	Coordinates (Angstroms) X	Y	Z
1	6	0	0.548118	-0.140868	0.000000
2	7	0	-0.868822	-0.293679	0.000000
3	6	0	1.029268	1.157384	0.000000
4	6	0	2.401795	1.355009	0.000000
5	6	0	3.257680	0.261578	0.000000
6	7	0	-1.520585	-1.245166	0.000000
7	7	0	-3.294866	-0.749919	0.000000
8	6	0	2.752455	-1.035996	0.000000
9	6	0	1.386004	-1.250654	0.000000
10	7	0	-3.119838	0.432935	0.000000
11	7	0	-2.639564	1.468839	0.000000
12	1	0	0.329703	1.981816	0.000000
13	1	0	2.800187	2.359441	0.000000
14	1	0	4.327543	0.418332	0.000000
15	1	0	3.426175	-1.881111	0.000000
16	1	0	0.970195	-2.248268	0.000000

***s-trans*-TS1**

Center Number	Atomic Number	Atomic Type	Coordinates (Angstroms) X	Y	Z
1	6	0	-0.905533	-0.085969	-0.000001
2	7	0	0.500679	-0.237355	-0.000002
3	6	0	-1.671048	-1.241845	0.000000
4	6	0	-3.049947	-1.111142	0.000000
5	6	0	-3.625882	0.152814	0.000001
6	7	0	1.465890	0.348946	-0.000003
7	7	0	3.001732	-0.911111	-0.000001
8	6	0	-2.834925	1.298853	0.000000
9	6	0	-1.456738	1.191833	0.000000
10	7	0	3.889264	-0.115761	0.000001
11	7	0	4.705264	0.684559	0.000003
12	1	0	-1.188012	-2.208160	-0.000001
13	1	0	-3.672104	-1.994330	0.000001
14	1	0	-4.702761	0.249693	0.000002
15	1	0	-3.294160	2.277064	0.000001
16	1	0	-0.818319	2.063532	-0.000001

***s-cis*-TS2**

Center Number	Atomic Number	Atomic Type	Coordinates (Angstroms) X	Y	Z
1	6	0	0.000000	0.624432	0.000000
2	7	0	0.182788	-0.781907	0.000000
3	6	0	1.164884	1.385511	0.000000
4	6	0	1.092282	2.771143	0.000000
5	6	0	-0.143295	3.403283	0.000000
6	7	0	-0.858698	-1.462269	0.000000
7	7	0	-0.835235	-2.735308	0.000000
8	6	0	-1.307257	2.640151	0.000000
9	6	0	-1.243771	1.256662	0.000000
10	7	0	0.568748	-3.220368	0.000000
11	7	0	1.388771	-3.942479	0.000000
12	1	0	2.119537	0.876375	0.000000
13	1	0	2.002423	3.355674	0.000000
14	1	0	-0.202613	4.483056	0.000000
15	1	0	-2.272631	3.128698	0.000000
16	1	0	-2.148395	0.665425	0.000000

***s-trans*-TS2**

Center Number	Atomic Number	Atomic Type	Coordinates (Angstroms) X	Y	Z
1	6	0	0.000000	0.928192	0.000000
2	7	0	-1.179476	0.138344	0.000000
3	6	0	-0.200821	2.305885	0.000000
4	6	0	0.882887	3.172513	0.000000
5	6	0	2.177171	2.670376	0.000000
6	7	0	-0.942189	-1.101200	0.000000
7	7	0	-1.913353	-1.887368	0.000000
8	6	0	2.377796	1.293454	0.000000
9	6	0	1.300545	0.422167	0.000000
10	7	0	-1.288084	-3.407273	0.000000
11	7	0	-1.333405	-4.495393	0.000000
12	1	0	-1.215386	2.682039	0.000000
13	1	0	0.713965	4.241048	0.000000
14	1	0	3.023972	3.342956	0.000000
15	1	0	3.383894	0.895189	0.000000
16	1	0	1.463629	-0.646519	0.000000

TSrot

Center Number	Atomic Number	Atomic Type	Coordinates (Angstroms) X	Y	Z
1	6	0	-1.243337	-1.128191	0.041795
2	6	0	-0.690398	0.129990	-0.192371
3	6	0	-1.480983	1.271192	-0.180530
4	6	0	-2.841119	1.161615	0.073014
5	6	0	-3.399200	-0.086399	0.307503
6	6	0	-2.600176	-1.227953	0.290298
7	7	0	0.693928	0.358609	-0.466503
8	7	0	1.402544	-0.630417	-0.423484
9	7	0	2.779175	-0.290302	-0.789538
10	7	0	3.400652	0.073888	0.210261
11	7	0	4.027776	0.400122	1.076068
12	1	0	-1.018215	2.230388	-0.369135
13	1	0	-3.460621	2.047498	0.084156
14	1	0	-4.459220	-0.175905	0.502830
15	1	0	-3.041945	-2.198444	0.470514
16	1	0	-0.617240	-2.008365	0.025766

TSsn2

Center Number	Atomic Number	Atomic Type	Coordinates (Angstroms) X	Y	Z
1	6	0	0.295376	-0.359268	-0.079997
2	7	0	-1.076378	-1.127576	-0.833783

3	6	0	1.225987	-1.222272	0.436492
4	6	0	2.522597	-0.726434	0.490833
5	6	0	2.827133	0.537056	-0.004851
6	7	0	-2.017993	-0.936643	-1.359398
7	6	0	1.833017	1.323770	-0.567972
8	6	0	0.517757	0.870352	-0.639901
9	1	0	0.959225	-2.200542	0.804733
10	1	0	3.297139	-1.349303	0.916437
11	1	0	3.843955	0.899840	0.033528
12	1	0	2.063397	2.302337	-0.966304
13	1	0	-0.279196	1.461090	-1.071026
14	7	0	-2.093529	0.534846	0.876474
15	7	0	-1.253105	-0.052826	1.459115
16	7	0	-2.875527	1.060392	0.211164

TS1per

Center Number	Atomic Number	Atomic Type	Coordinates (Angstroms) X	Y	Z
1	7	0	1.278541	-2.757075	0.000000
2	7	0	0.249766	-3.218452	0.000000
3	7	0	-1.023970	-2.909626	0.000000
4	7	0	-1.061186	-1.522249	0.000000
5	7	0	-0.002183	-0.920968	0.000000
6	6	0	0.000000	0.498587	0.000000
7	6	0	1.250118	1.102508	0.000000
8	6	0	1.341244	2.486544	0.000000
9	6	0	0.186512	3.257050	0.000000
10	6	0	-1.062470	2.642881	0.000000
11	6	0	-1.165302	1.262591	0.000000
12	1	0	2.134522	0.479757	0.000000
13	1	0	2.312779	2.960954	0.000000
14	1	0	0.256394	4.336180	0.000000
15	1	0	-1.961042	3.244653	0.000000
16	1	0	-2.130050	0.776075	0.000000

TS2per

Center Number	Atomic Number	Atomic Type	Coordinates (Angstroms) X	Y	Z
1	6	0	0.408497	-0.016698	-0.163394
2	7	0	-0.993207	0.031457	-0.311051
3	6	0	1.102090	1.177826	-0.315999
4	6	0	2.477451	1.185560	-0.144152
5	6	0	3.154191	0.009397	0.153010
6	7	0	-1.766850	-0.965657	-0.430779

7	7	0	-2.925296	-0.936167	-0.157132
8	6	0	2.448448	-1.179328	0.291068
9	6	0	1.070004	-1.200329	0.147141
10	7	0	-3.054738	0.698943	0.464192
11	7	0	-2.011252	1.192115	0.427932
12	1	0	0.563166	2.081487	-0.564072
13	1	0	3.021364	2.113401	-0.255112
14	1	0	4.228306	0.017997	0.275135
15	1	0	2.970706	-2.097766	0.521345
16	1	0	0.511777	-2.118527	0.264522

Full reference 18

Gaussian 09, Revision B.01, M. J. Frisch, G. W. Trucks, H. B. Schlegel, G. E. Scuseria, M. A. Robb, J. R. Cheeseman, G. Scalmani, V. Barone, B. Mennucci, G. A. Petersson, H. Nakatsuji, M. Caricato, X. Li, H. P. Hratchian, A. F. Izmaylov, J. Bloino, G. Zheng, J. L. Sonnenberg, M. Hada, M. Ehara, K. Toyota, R. Fukuda, J. Hasegawa, M. Ishida, T. Nakajima, Y. Honda, O. Kitao, H. Nakai, T. Vreven, J. A. Montgomery, Jr., J. E. Peralta, F. Ogliaro, M. Bearpark, J. J. Heyd, E. Brothers, K. N. Kudin, V. N. Staroverov, T. Keith, R. Kobayashi, J. Normand, K. Raghavachari, A. Rendell, J. C. Burant, S. S. Iyengar, J. Tomasi, M. Cossi, N. Rega, J. M. Millam, M. Klene, J. E. Knox, J. B. Cross, V. Bakken, C. Adamo, J. Jaramillo, R. Gomperts, R. E. Stratmann, O. Yazyev, A. J. Austin, R. Cammi, C. Pomelli, J. W. Ochterski, R. L. Martin, K. Morokuma, V. G. Zakrzewski, G. A. Voth, P. Salvador, J. J. Dannenberg, S. Dapprich, A. D. Daniels, O. Farkas, J. B. Foresman, J. V. Ortiz, J. Cioslowski, and D. J. Fox, Gaussian, Inc., Wallingford CT, 2010.